Video Article

Electron Channeling Contrast Imaging for Rapid III-V Heteroepitaxial Characterization

Julia I. Deitz[1], Santino D. Carnevale[2], Steven A. Ringel[3], David W. McComb[3], Tyler J. Grassman[1,2]

[1]Department of Materials Science and Engineering, The Ohio State University

[2]Department of Electrical and Computer Engineering, The Ohio State University

[3]Institute of Materials Research, The Ohio State University

Correspondence to: Tyler J. Grassman at grassman.5@osu.edu

URL: http://www.jove.com/video/52745
DOI: doi:10.3791/52745

Keywords: Engineering, Issue 101, Electron channeling contrast imaging, ECCI, electron microscopy, lattice-mismatch, misfit dislocations, semiconductors, heterostructures, rapid characterization

Date Published: 7/17/2015

Citation: Deitz, J.I., Carnevale, S.D., Ringel, S.A., McComb, D.W., Grassman, T.J. Electron Channeling Contrast Imaging for Rapid III-V Heteroepitaxial Characterization. *J. Vis. Exp.* (101), e52745, doi:10.3791/52745 (2015).

Abstract

Misfit dislocations in heteroepitaxial layers of GaP grown on Si(001) substrates are characterized through use of electron channeling contrast imaging (ECCI) in a scanning electron microscope (SEM). ECCI allows for imaging of defects and crystallographic features under specific diffraction conditions, similar to that possible via plan-view transmission electron microscopy (PV-TEM). A particular advantage of the ECCI technique is that it requires little to no sample preparation, and indeed can use large area, as-produced samples, making it a considerably higher throughput characterization method than TEM. Similar to TEM, different diffraction conditions can be obtained with ECCI by tilting and rotating the sample in the SEM. This capability enables the selective imaging of specific defects, such as misfit dislocations at the GaP/Si interface, with high contrast levels, which are determined by the standard invisibility criteria. An example application of this technique is described wherein ECCI imaging is used to determine the critical thickness for dislocation nucleation for GaP-on-Si by imaging a range of samples with various GaP epilayer thicknesses. Examples of ECCI micrographs of additional defect types, including threading dislocations and a stacking fault, are provided as demonstration of its broad, TEM-like applicability. Ultimately, the combination of TEM-like capabilities – high spatial resolution and richness of microstructural data – with the convenience and speed of SEM, position ECCI as a powerful tool for the rapid characterization of crystalline materials.

Video Link

The video component of this article can be found at http://www.jove.com/video/52745/

Introduction

Detailed characterization of crystalline defects and microstructure is a vitally important aspect of semiconductor materials and device research since such defects can have a significant, detrimental impact on device performance. Currently, transmission electron microscopy (TEM) is the most widely accepted and used technique for detailed characterization of extended defects – dislocations, stacking faults, twins, antiphase domains, etc. – because it enables the direct imaging of a wide variety of defects with ample spatial resolution. Unfortunately, TEM is a fundamentally low-throughput approach due to lengthy sample preparation times, which can lead to significant delays and bottlenecks in research and development cycles. Additionally, the integrity of the sample, such as in terms of the as-grown strain state, can be altered during sample preparation, leaving the opportunity for adulterated results.

Electron channeling contrast imaging (ECCI) is a complementary, and in some cases a potentially superior, technique to TEM as it provides an alternative, high-throughput approach for imaging the same extended defects. In the case of epitaxial materials, samples need little to no preparation, making ECCI much more time efficient. Additionally advantageous is the fact that ECCI requires only a field-emission scanning electron microscope (SEM) equipped with a standard annular pole-piece mounted backscatter electron (BSE) detector; forescatter geometry can also be used, but requires slightly more specialized equipment and is not discussed here. The ECCI signal is composed of electrons that have been inelastically scattered out of the in-going channeled beam (electron wave-front), and through multiple additional inelastic scattering events, are able escape the sample back through the surface.[1] Similar to two-beam TEM, it is possible to perform ECCI at specific diffraction conditions in the SEM by orienting the sample so that the incident electron beam satisfies a crystallographic Bragg condition (*i.e.,* channeling), as determined using low-magnification electron channeling patterns (ECPs);[1,2] see **Figure 1** for an example. Simply, ECPs provide an orientation-space representation of incident electron beam diffraction/channeling.[3] Dark lines resulting from low backscatter signal indicate beam-sample orientations where Bragg conditions are met (*i.e.*, Kikuchi lines), which yields strong channeling, whereas the bright regions indicate high backscatter, non-diffractive conditions. As opposed to Kikuchi patterns produced via electron backscatter diffraction (EBSD) or TEM, which are formed via *outgoing* electron diffraction, ECPs are a result of *incident* electron diffraction/channeling.

In practice, controlled diffraction conditions for ECCI are achieved by adjusting the sample orientation, via tilt and/or rotation under low magnification, such that the ECP feature representing the well-defined Bragg condition of interest – for example, a [400] or [220] Kikuchi

band/line – is coincident with the optic axis of the SEM. Transitioning to high magnification then, because of the resultant restriction of the angular range of the incident electron beam, effectively selects for a BSE signal that ideally corresponds only to scattering from the chosen diffraction condition. In this manner it is possible to observe defects that provide diffraction contrast, such as dislocations. Just as in TEM, the imaging contrast presented by such defects is determined by the standard invisibility criteria, $\mathbf{g} \cdot (\mathbf{b} \times \mathbf{u}) = 0$ and $\mathbf{g} \cdot \mathbf{b} = 0$, where **g** represents the diffraction vector, **b** the Burgers vector, and **u** the line direction.[4] This phenomenon occurs because only diffracted electrons from planes distorted by the defect will contain information about said defect.

To date, ECCI has predominantly been used to image features and defects near or at the sample surface for such functional materials as GaSb,[5] $SrTiO_3$,[5] GaN,[6-9] and SiC.[10,11] This limitation is the result of the surface-sensitive nature of the ECCI signal itself, wherein the BSE that make up the signal come from a depth range of about 10 – 100 nm. The most significant contribution to this depth resolution limit is that of broadening and damping of the in-going electron wave front (channeled electrons), as a function of depth into the crystal, due to the loss of electrons to scattering events, which reduces the maximum potential BSE signal.[1] Nonetheless, some degree of depth resolution has been reported in previous work on $Si_{1-x}Ge_x$/Si and $In_xGa_{1-x}As$/GaAs heterostructures,[12,13] as well as more recently (and herein) by the authors on GaP/Si heterostructures,[14] where ECCI was used to image misfit dislocations buried at the lattice-mismatched heteroepitaxial interface at depths of up to 100 nm (with higher depths likely possible).

For the work detailed here, ECCI is used to study GaP epitaxially grown on Si(001), a complex materials integration system with application toward such areas as photovoltaics and optoelectronics. GaP/Si is of particular interest as a potential pathway for the integration of metamorphic (lattice-mismatched) III-V semiconductors onto cost-effective Si substrates. For many years efforts in this direction have been plagued by the uncontrolled generation of large numbers of heterovalent nucleation related defects, including antiphase domains, stacking faults, and microtwins. Such defects are detrimental to device performance, especially photovoltaics, due to the fact that they can be electrically active, acting as carrier recombination centers, and can also hinder interfacial dislocation glide, leading to higher dislocation densities.[15] However, recent efforts by the authors and others have led to the successful development of epitaxial processes that can produce GaP-on-Si films free of these nucleation related defects,[16-19] thereby paving the way for continued progress.

Nonetheless, because of the small, but non-negligible, lattice mismatch between GaP and Si (0.37% at RT), the generation of misfit dislocations is unavoidable, and indeed necessary to produce fully relaxed epilayers. GaP, with its FCC-based zinc blende structure, tends to yield 60° type dislocations (mixed edge and screw) on the slip system, which are glissile and can relieve large amounts of strain through long net glide lengths. Additional complexity is also introduced by the mismatch in GaP and Si thermal expansion coefficients, which results in an increasing lattice mismatch with increasing temperature (*i.e.*, ≥ 0.5% misfit at typical growth temperatures).[20] Because the threading dislocation segments that make up the remainder of the misfit dislocation loop (along with the interfacial misfit and the crystal surface) are well known for their associated non-radiative carrier recombination properties, and thus degraded device performance,[21] it is important to fully understand their nature and evolution such that their numbers can be minimized. Detailed characterization of the interfacial misfit dislocations can thus provide a substantial amount of information about the dislocation dynamics of the system.

Here, we describe the protocol for using an SEM to perform ECCI and provide examples of its capabilities and strengths. An important distinction here is the use of ECCI to perform microstructural characterization of the sort typically performed via TEM, whereas ECCI provides the equivalent data but in a significantly shorter time frame due to the significantly reduced sample preparation needs; in the case for epitaxial samples with relatively smooth surfaces, there is effectively no sample preparation required at all. The use of ECCI for general characterization of defects and misfit dislocations is described, with some examples of observed crystalline defects provided. The impact of invisibility criteria on the observed imaging contrast of an array of interfacial misfit dislocations is then described. This is followed by a demonstration of how ECCI can be used to perform important modes of characterization – in this case a study to determine the GaP-on-Si critical thickness for dislocation nucleation – providing TEM-like data, but from the convenience of an SEM and in significantly reduced time frame.

Protocol

This protocol was written with an assumption that the reader will have a working understanding of standard SEM operation. Depending upon the manufacturer, model, and even software version, every SEM can have significantly different hardware and/or software interfaces. The same can be said with respect to the internal configuration of the instrument; the operator must be cautious and observant when following this protocol, as even relatively small changes in sample size/geometry, sample orientation (tilt, rotation), and working distance, can present a risk for making contact with the pole–piece, especially if not at eucentric height. The instructions provided here are for the instrument used to perform this work, a FEI Sirion SEM equipped with a field emission gun and a standard, pole-piece mounted, annular Si backscatter detector. Therefore, it is imperative that the reader understand how to perform the equivalent actions on their own specific equipment.

1. Sample Preparation

1. Cleave sample, GaP/Si for this study, into a suitable size depending on the size of the SEM sample mount that is to be used. Note: The sample can be as small as 5 mm x 5 mm or as large as a full wafer (4 inches long), depending on the internal geometry of the SEM used and the available chamber space.The sample surface should be very clean and free of contamination that could disturb the channeling (*e.g.*, crystalline or amorphous native oxides).
2. Place the sample onto the SEM sample mount. Note: The mounting method may change depending on the type of SEM stub used, typically either a clip style or via some adhesive (*e.g.*, carbon tape, silver paint). The method of placement must ensure that the sample will not move and that it is electrically grounded to prevent sample charging.

2. Load Sample

1. Vent the SEM by clicking the 'Vent' button in the software interface and insert the sample after reaching atmospheric pressure.

2. Before closing the SEM door, ensure that the sample is at an appropriate height so as to not strike the BSE detector upon moving into the SEM.
3. Pump down the SEM by clicking the 'Pump' button in the software interface. Wait until system indicates that the pressure is low enough to start the measurements.

3. Set Appropriate Working Conditions

1. Turn on the electron beam via the control button in the 'Beam' control area and set the accelerating voltage via the 'Beam' drop-down menu in the software interface. For the work presented here, 25 kV was used.
2. Set the beam current to an appropriate value via 'Beam' drop-down menu. This is determined within the system used here by way of the spot size setting, which was set to 5 (approximately 2.4 nA). Note: High beam current is typically necessary because the ECCI signal is generally weak and larger current allows for a more distinguishable image.
3. Using the secondary electron detector, adjust the image focus and stigmation via the software interface. Note: This is performed here by right-clicking and dragging the mouse on the software interface; vertical for focus, horizontal for stigmation. Also, it is usually helpful to find a small particle or surface feature on the sample to provide a clear subject for focus/stigmation adjustment.
4. Move the sample into the vertical working distance by incrementally changing the Z position of the stage and adjusting the focus and stigmation as needed. The Z position is changed through the 'Z' drop-down menu in the 'Stage' control area of the software interface. For the work described here, a working distance of 5 mm placed the same at eucentric height and provided for a strong ECCI signal.

4. Visualize Sample ECP

1. Switch into BSE mode through the 'Detectors' drop-down menu in the software interface.
2. Decrease magnification to its lowest setting (27x), which is done here via the computer keyboard minus (-) key, to visualize the ECP.
3. Adjust the scan rate, done here via the 'Scan' drop-down menu, to provide an image with sufficient signal-to-noise (*e.g.*, slow scan rather than TV mode). Note: Averaging or integrating the image may be necessary to obtain a clearer, more discernable image.
4. Adjust the image contrast and brightness, accomplished here via the 'Contrast' and 'Brightness' sliders, to help enhance the visibility of the ECP, being careful not to oversaturate.
5. Adjust the sample rotation and tilt, using the 'R' and 'T' entries in the 'Stage' control area in the software interface, to help make features of the channeling pattern more apparent. Sample rotation will result in a rotation of the ECP (as shown in **Figure 2**) and tilting will result in a translation of the ECP (as shown in Figure 3).

5. Image Defects/Features

1. Adjust sample tilt and rotation, as described in step 4.5, to set the desired diffraction condition. Accomplish this by translating and/or rotating the ECP to align the target Kikuchi band edge (*i.e.*, inflection point between the bright Kikuchi band and its associated dark Kikuchi line) with the SEM optic axis. While maximum channeling actually occurs at the Kikuchi line, aligning in the method described here provides visualization contrast for defects with both dark and bright contrast levels (see **Figures 4 and 5**).
2. Once the desired diffraction condition is achieved, increase magnification, done here via the keyboard plus (+) key.
3. Refocus image and adjust for stigmation, as described in step 3.2. Note: Here, the focus and stigmation is best adjusted with respect to the specific defect/feature being imaged.
4. Because small deviations from the edge of the band can make large differences in the appearance of the target defect or feature, optimize the diffraction condition by making small (no more than adjustments to the sample tilt orthogonally to the Kikuchi band/line of interest, while watching a specific feature for maximum contrast. Note that moving toward the inside of the Kikuchi band will typically reduce the relative contrast of "bright" features, while moving toward the outside of the band (toward the Kikuchi line) will typically reduce the relative contrast of "dark" features.
5. Once the desired contrast is obtained, decrease the magnification to verify that the same band is still on or very near the optic axis; too much tilt can change the diffraction condition altogether.

Representative Results

The GaP/Si samples for this study were grown by metal-organic chemical vapor deposition (MOCVD) in an Aixtron 3×2 close-coupled showerhead reactor following the authors' previously reported heteroepitaxial process.[17] All growths were performed on 4 inch Si(001) substrates with intentional misorientation (offcut) of 6° toward [110]. All ECCI imaging was performed on as-grown samples with no further sample preparation whatsoever (aside from cleaving to yield approximately 1 cm x 1cm pieces for loading into the SEM).

Images of the misfit network in the GaP/Si sample captured under different diffraction conditions are shown in **Figure 4**. As indicated in **Figure 4A**, the position on the ECP map will determine the observed contrast of the defects, as determined by the invisibility criteria.

Figure 5 presents images captured from various GaP/Si samples with different GaP thicknesses in order to determine the critical thickness. These samples were all grown at 550 °C, which yields a lattice mismatch of approximately 0.47%. Using a **g** = imaging condition, misfit dislocations are not observed at 30 nm, but are observed at 50 nm, indicating that the critical thickness is somewhere in the range of 30 – 50 nm.

Finally, ECCI is used to image threading dislocations and a stacking fault (see **Figure 6**) **g** = diffraction condition to demonstrate applicability of ECCI to other types of defect characterization.

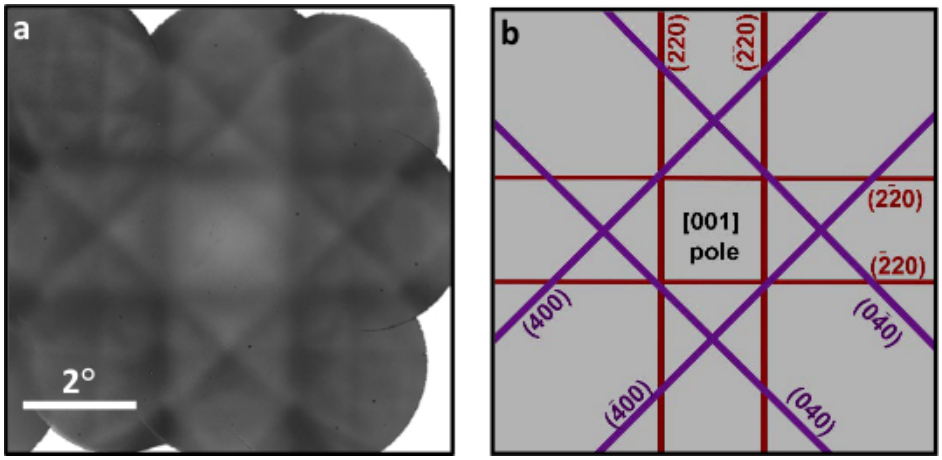

Figure 1. Experimental and Illustration of Electron Channeling Pattern (ECP). (**A**) Montage of captured ECP images (taken at 27x magnification) from a GaP/Si sample, along with (**B**) an indexed illustration describing the observable Kikuchi lines. Please click here to view a larger version of this figure.

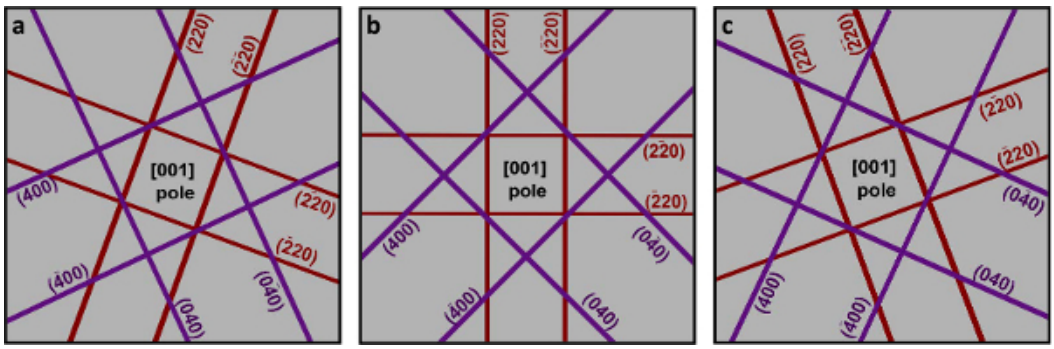

Figure 2. Rotation of Electron Channeling Pattern (ECP). Depiction of the effect of in-plane sample rotation (*i.e.*, about the [001] surface normal) on the appearance of the GaP/Si ECP. Rotations of (**A**) -20°, (**B**) 0°, and (**C**) 20° are shown. Please click here to view a larger version of this figure.

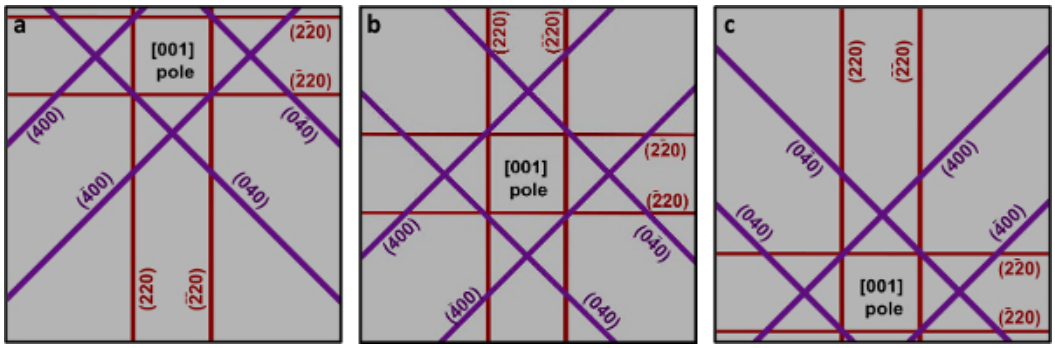

Figure 3. Tilt of Electron Channeling Pattern (ECP). Depiction of the effect of out-of-plane sample tilt (*i.e.*, about the in-plane [110]) on the appearance of the GaP/Si ECP. Tilts of (**A**) -4°, (**B**) 0°, and (**C**) 4° are shown. Please click here to view a larger version of this figure.

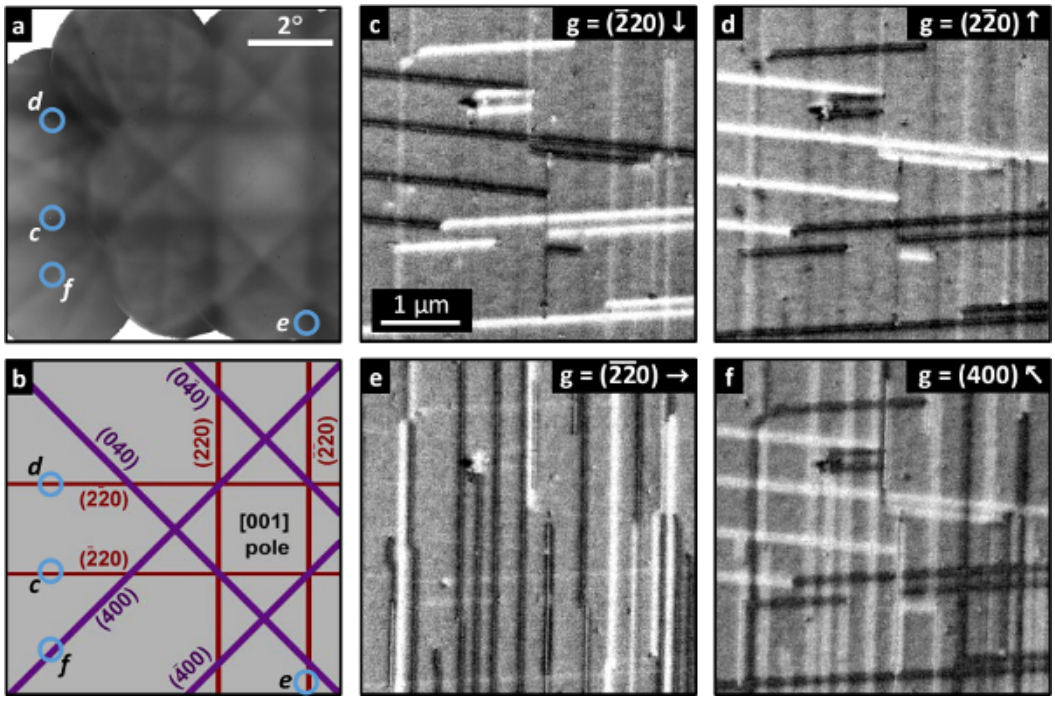

Figure 4. Annotated Electron Channeling Pattern (ECP) with Relative Image Results. (**A**) Montage of captured ECP images (27x magnification) and (**B**) indexed illustration indicating the relative positions of the optic axis used to produce the imaging conditions of the ECCI images displayed in (**C**) – (**F**), which show misfit dislocations at the lattice-mismatched interface of a 50 nm thick GaP/Si sample. Respective **g** vectors are indicated for each image. Adapted with permission from [14]. Please click here to view a larger version of this figure.

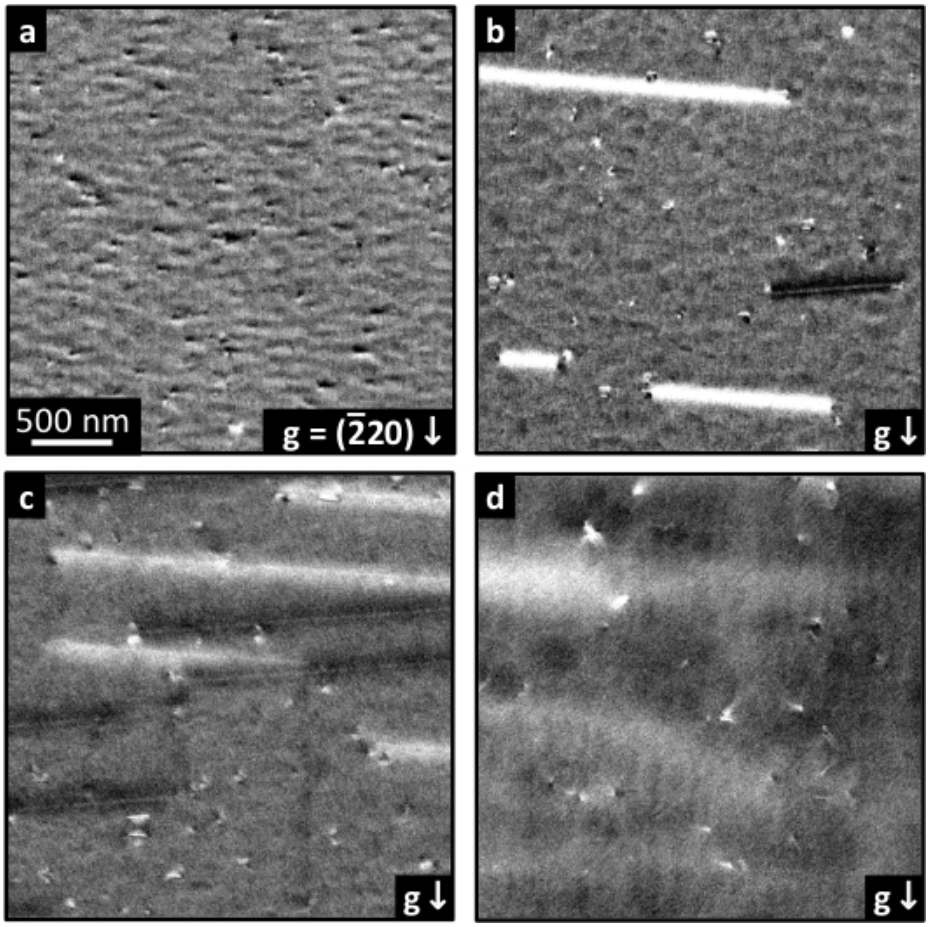

Figure 5. GaP/Si Thickness Series. ECCI micrographs from a GaP/Si thickness series, including (**A**) 30 nm, (**B**) 50 nm, (**C**) 100 nm, and (**D**) 250 nm GaP epilayer thicknesses. Misfit dislocations are observable beginning with the 50 nm sample, indicating that the critical thickness is somewhere between 30 nm and 50 nm. Adapted with permission from [14]. Please click here to view a larger version of this figure.

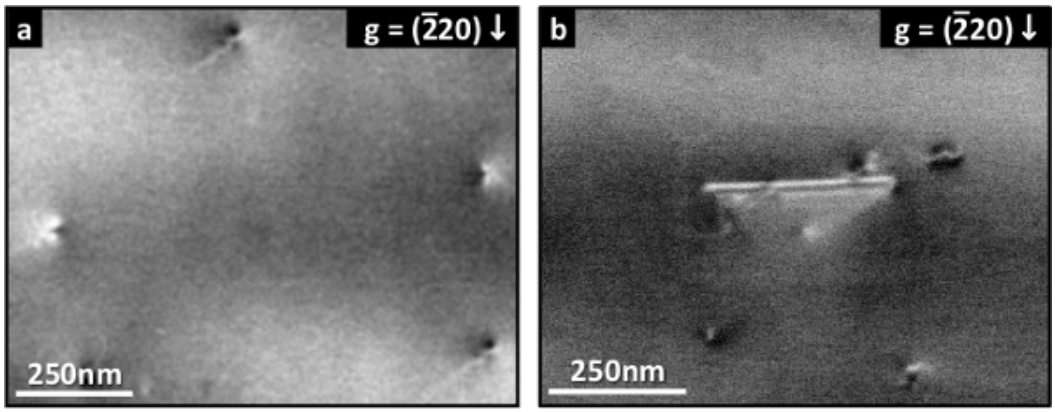

Figure 6. Additional Defects Taken with Electron Channeling Contrast Imaging (ECCI). ECCI images of additional defect types in different GaP/Si samples, including (**A**) surface penetrating threading dislocations and (**B**) a stacking fault. Please click here to view a larger version of this figure.

Discussion

An accelerating voltage of 25 kV was used for this study. The accelerating voltage will determine the electron beam penetration depth; with higher accelerating voltage, there will be BSE signal coming from greater depths in the sample. The high accelerating voltage was chosen for this system because it allows for visibility of dislocations that are far from the surface of the sample, buried at the interface. Other types of defects/features may be more or less visible at different accelerating voltages depending on the type of sample.

As previously discussed, the invisibility criteria will determine what features have strong contrast at the specific diffraction condition in use and the resultant imaging contrast of those features. Just as in TEM, this can be used to provide guidance to the operator as to what imaging

conditions will be necessary to observe the particular defects of interest, or in the case of some unknown defect, a range of different diffraction conditions can be used to provide further information to help elucidate the nature of that defect. For example, to clearly image an array of misfit dislocations (MDs) that are orthogonal to each other, a number of different diffraction conditions can be used, depending upon the goal of the operator. This was previously demonstrated by the authors for ECCI characterization of MDs in GaP/Si,[14] and is shown here in **Figure 4** where four images of the same MD network, taken from a 50 nm thick GaP/Si sample, were captured using different diffraction conditions.

Figure 4A presents an ECP map indicating the diffraction condition, g, used in each of the images displayed in **Figure 4B-E**. **Figure 4B** is an image of the MD network as imaged under the g = $\bar{2}$20] condition. As previously discussed, dislocation contrast is determined by the invisibility criteria, g · b = 0 and g · (b x u) = 0. In (001)-oriented zinc blende crystals, compressive strain is relieved by dislocations with u = $\bar{1}$10] and $\bar{1}$10] line directions – vertical and horizontal, respectively, in the coordinates of **Figure 4** – with four distinct Burgers vectors possible for each. For the g = [$\bar{2}$20] diffraction condition all four possible Burgers vectors associated with the horizontal u = $\bar{1}\bar{1}$0] line direction give non-zero values for both invisibility criteria and thus provide strong contrast. Those on the vertical u = $\bar{1}$10] direction yield g · (b × u) = 0, but also g · b ≠ 0, and should thus provide only weak contrast, as can be seen in **Figure 4B**. Note that the off-axis tilt of the dislocations in the horizontal direction is a result of the use of an intentionally misoriented Si(001) substrate (*i.e.*, offcut 6° toward [110]).[22] The opposite contrast levels displayed by the horizontal MDs (*i.e.*, dark and bright) are related to the sign of g · (b × u), thereby providing an additional level of distinction between the different dislocations. Previous work by the authors comparing experimental and simulated offcut GaP/Si ECCI data indicated that of the four possible Burgers vectors for the u = $\bar{1}$10] (horizontal) line direction, only two are actually observed, potentially due to a preferential dislocation nucleation and glide mechanism resulting from the offcut substrate;[23] whether the same occurs in the u = $\bar{1}$10] (vertical) direction is difficult to ascertain due to the lack of offcut induced dislocation skew.

Figure 4C shows the same MD network with the diffraction condition antiparallel to that of **Figure 4B**, g = [$\bar{2}$20]. Because the dislocations that are perpendicular to g = $\bar{2}$20] are also perpendicular to g = [$\bar{2}$20], they still possess high contrast, but with opposite polarity due to the change in sign of the diffraction condition. This means that contrast reversal can be used in combination with the standard invisibility criteria using a set of known g vectors to determine the sign of the Burgers vector of a given defect. Indeed, the **Figure 4B and 4C** images were taken using the same Kikuchi band, but on opposite edges. In Fig. 4(d), the vertical oriented MDs, which are orthogonal to those highlighted in **Figure 4B-C** now exhibit strong contrast due to the use of an orthogonal diffraction vector, g = [220], while the horizontal dislocations exhibit very weak contrast. Finally, in **Figure 4E**, both sets of MDs are visible when using the diffraction condition g = [400], which is non-parallel to either set and thus yields non-zero invisibility criteria values for all the possible Burgers vectors and line directions.

In addition to providing TEM-like data within an SEM, a particular strength of ECCI is the ability to perform some such analyses in a rapid manner, significantly faster and simpler than would typically be possible via TEM. One example of this is presented in **Figure 5**, where ECCI was used to perform a multi-sample analysis of misfit dislocation evolution over a range of GaP-on-Si film thicknesses (30 nm to 250 nm), with the goal of accurately determining the critical thickness (the thickness necessary to induced strain relaxation via the formation of dislocations) for dislocation nucleation, h_c, as well as developing a better understanding of dislocation glide dynamics. **Figure 5A** shows an ECCI image of a 30 nm thick sample, which exhibits no observable MD features. This thickness is thus most likely sufficiently below h_c such that no nucleation events have yet occurred. This is consistent with previous TEM-based studies suggesting that the GaP-on-Si h_c is somewhere in the range of 45nm – 90nm.[24,25] However, it is possible that some nucleation events have actually occurred but have not yet produced any observable misfit length. In this case, the just-nucleated dislocations should still be observable – indeed, there are a number of contrast features in the image that could be related to this, or to a slight surface roughness – but may be difficult to adequately resolve due to a lack of strain-driven loop expansion.

As the film thickness increases, presented in **Figure 5B** (50 nm) and **Figure 5C** (100 nm), interfacial misfit segments are seen to appear and extend, relieving excess misfit strain via glide; the thicker the epilayer the longer the resultant misfit lengths and the greater the number of MDs visible. The appearance of observable misfit dislocations in the 50 nm sample, **Figure 5B**, indicates that the critical thickness has been reached (at least at the growth temperature), giving a critical thickness estimate of somewhere in the range of about 30 nm – 50 nm, which represents a significant narrowing, and perhaps a slight shift, of the previously reported range. Additional high-temperature (725°C) annealing experiments (not shown here) were found to yield observable, though short, misfit lengths in the 30 nm the nucleation,[14] suggesting that the critical thickness value may actually closer to the lower limit or mid-range. At significantly higher GaP thickness, such as the 250 nm sample shown in **Figure 5D**, the MDs themselves are no longer directly observable due to the previously mentioned depth-dependent broadening/damping of the ingoing electron wave front. Instead, the associated near-surface threading segments are visible, as well as broad contrast features likely related to misfit dislocation induced heterogeneous strain fields. This ability to non-destructively observe and count threading dislocations in such films at TEM-like spatial resolutions, which typically requires time-consuming plan-view TEM foil preparation and yields comparatively small areas of analysis, is another important strength of the ECCI technique.

While the main focus in this paper is the use of ECCI to characterize misfit dislocations in GaP/Si, it is important to note that it can also be applied to the characterization of other crystalline materials and other types of defects. **Figure 6** presents examples of the latter. **Figure 5A** displays an ECCI micrograph of surface-penetrating threading dislocations in a 250 nm thick GaP-on-Si(001) sample, taken at higher resolution than that of **Figure 5D**. Of note here is that even the fringed tail of the thread can be seen, a feature regularly observed via plan-view geometry TEM (PV-TEM). Similarly, **Figure 6B** displays an ECCI micrograph of a stacking fault in the same sample – an important tell-tale sign of non-optimal GaP nucleation for this particular test structure – which also displays observable extinction fringes. This fringing has also been observed via ECCI in metals samples by other researchers.[1,26] These types of micrographs can be obtained via ECCI much more quickly than via TEM since the sample requires no preparation or processing. All the while, the potential resolution achievable with ECCI is comparable to that of conventional PV-TEM, making ECCI an effective tool for rapid characterization of density and distribution of extended defects, such as dislocations and stacking faults, as demonstrated above.

In this work the procedure for ECCI was described. Because the ECCI signal is diffraction-based, it can be performed under different, specific diffraction conditions much in the same way the TEM operates, making it possible to image various types of defects. This makes ECCI an excellent alternative to TEM for detailed microstructural characterization in cases where rapid turn-around and/or large numbers of samples are needed, or where non-destructive, wide-area characterization is desired. Here, ECCI was demonstrated through the characterization of misfit dislocations at the lattice-mismatched interface of heteroepitaxial GaP-on-Si samples, but it has a large range of applicability and can be used for other types of defects and crystalline structures.

Disclosures

The authors have nothing to disclose.

Acknowledgements

This work was supported by the Department of Energy under the FPACE program (DE-EE0005398), the Ohio State University Institute for Materials Research, and the Ohio Office of Technology Investments' Third Frontier Program.

References

1. Zaefferer, S., Elhami, Theory and application of electron channelling contrast imaging under controlled diffraction conditions. *Acta Mater.* **75**, 20-50 (2014).
2. Crimp, M. A. Scanning electron microscopy imaging of dislocations in bulk materials, using electron channeling contrast. *Microsc. Res. Tech.* **69**, (5), 374-381 (2006).
3. Joy, D. C., Newbury, D. E., Davidson, D. L. Electron channeling patterns in the scanning electron microscope. *J. Appl. Phys.* **53**, (8), R81-R122 (1982).
4. Williams, D. B., Carter, C. B. *Transmission Electron Microscopy: A Textbook for Materials Science.* Springer New York (2009).
5. Picard, Y. N., *et al.* Future Prospects for Defect and Strain Analysis in the SEM via Electron Channeling. *Micros. Today.* **20**, (2), 12-16 (2012).
6. Naresh-Kumar, G., *et al.* Rapid Nondestructive Analysis of Threading Dislocations in Wurtzite Materials Using the Scanning Electron Microscope. *Phys. Rev. Lett.* **108**, (13), 135503 (2012).
7. Naresh-Kumar, G., *et al.* Electron channeling contrast imaging studies of nonpolar nitrides using a scanning electron microscope. *Appl. Phys. Lett.* **102**, (14), 142103 (2013).
8. Kamaladasa, R. J., *et al.* Identifying threading dislocations in GaN films and substrates by electron channelling. *J. Microsc.* **244**, (3), 311-319 (2011).
9. Picard, Y. N., *et al.* Nondestructive analysis of threading dislocations in GaN by electron channeling contrast imaging. *Appl. Phys. Lett.* **91**, (9), 094106 (2007).
10. Picard, Y. N., *et al.* Electron channeling contrast imaging of atomic steps and threading dislocations in 4H-SiC. *Appl. Phys. Lett.* **90**, (23), 234101 (2007).
11. Picard, Y., *et al.* Epitaxial SiC Growth Morphology and Extended Defects Investigated by Electron Backscatter Diffraction and Electron Channeling Contrast Imaging. *J. Electron. Mater.* **37**, (5), 691-698 (2008).
12. Wilkinson, A. J. Observation of strain distributions in partially relaxed In0.2Ga0.8As on GaAs using electron channelling contrast imaging. *Philos. Mag. Lett.* **73**, (6), 337-344 (1996).
13. Wilkinson, A. J., Anstis, G. R., Czernuszka, J. T., Long, N. J., Hirsch, P. B. Electron Channeling Contrast Imaging of Interfacial Defects in Strained Silicon-Germanium Layers on Silicon. *Philos. Mag. A.* **68**, (1), 59-80 (1993).
14. Carnevale, S. D., *et al.* Rapid misfit dislocation characterization in heteroepitaxial III-V/Si thin films by electron channeling contrast imaging. *Appl. Phys. Lett.* **104**, (23), 232111 (2014).
15. Kvam, E. Interactions of dislocations and antiphase (inversion) domain boundaries in III–V/IV heteroepitaxy. *J. Electron. Mater.* **23**, (10), 1021-1026 (1994).
16. Grassman, T. J., *et al.* Control and elimination of nucleation-related defects in GaP/Si(001) heteroepitaxy. *Appl. Phys. Lett.* **94**, (23), 232106 (2009).
17. Grassman, T. J., *et al.* Nucleation-related defect-free GaP/Si(100) heteroepitaxy via metal-organic chemical vapor deposition. *Appl. Phys. Lett.* **102**, (14), 142102 (2013).
18. Volz, K., *et al.* GaP-nucleation on exact Si(001) substrates for III/V device integration. *J. Cryst. Growth.* **315**, (1), 37-47 (2011).
19. Beyer, A., *et al.* GaP heteroepitaxy on Si(001): Correlation of Si-surface structure, GaP growth conditions, and Si-III/V interface structure. *J. Appl. Phys.* **111**, (8), 083534 (2012).
20. *Thermal Expansion: Nonmetallic Solids.* Touloukian, Y. S. IFI/Plenum New York (1977).
21. Yamaguchi, M. Dislocation density reduction in heteroepitaxial III-V compound films on Si substrates for optical devices. *J. Mater. Res.* **6**, (2), 376-384 (1991).
22. Nemanich Ware, R. J., Gray, J. L., Hull, R. Analysis of a nonorthogonal pattern of misfit dislocation arrays in SiGe epitaxy on high-index Si substrates. *J. Appl. Phys.* **95**, (1), 115-122 (2004).
23. Ghandhi Ayers, S. K., Schowalter, L. J. Crystallographic tilting of heteroepitaxial layers. *J. Cryst. Growth.* **113**, (3-4), 430-440 (1991).
24. Yamane, T., Kawai, Y., Furukawa, H., Okada, A. Growth of low defect density GaP layers on Si substrates within the critical thickness by optimized shutter sequence and post-growth annealing. *J. Cryst. Growth.* **312**, (15), 2179-2184 (2010).
25. Jimbo Soga, T., Umeno, M. Dislocation Generation Mechanisms For GaP On Si Grown By Metalorganic Chemical-Vapor-Deposition. *Appl. Phys. Lett.* **63**, (18), 2543-2545 (1993).
26. Weidner, A., Martin, S., Klemm, V., Martin, U., Biermann, H. Stacking faults in high-alloyed metastable austenitic cast steel observed by electron channelling contrast imaging. *Scripta Mater.* **64**, (6), 513-516 (2011).

